A novel hybrid trust region minimax fitting algorithm for accurate dimensional metrology of aspherical shapes

Yassir Arezki, Hichem Nouira, Nabil Anwer, Charyar Mehdi-Souzani

Measurement 127 (2018) 134–140

Contents lists available at ScienceDirect

Measurement

journal homepage: www.elsevier.com/locate/measurement

A novel hybrid trust region minimax fitting algorithm for accurate dimensional metrology of aspherical shapes

Yassir Arezki[a,b,*], Hichem Nouira[a,*], Nabil Anwer[b], Charyar Mehdi-Souzani[b]

[a] Laboratoire Commun de Métrologie (LCM), Laboratoire National de Métrologie et d'Essais (LNE), 1 Rue Gaston Boissier, 75015 Paris, France
[b] LURPA, ENS Cachan, Univ. Paris-Sud, Université Paris-Saclay, 94235 Cachan, France

ARTICLE INFO

Keywords:
Trust region methods
Aspheric shapes
Minimax
Chebyshev fitting
Minimization
Form error
Dimensional metrology
Ultra-high precision engineering

ABSTRACT

Ultra-high precision measuring machines enable to measure aspheric shapes with an uncertainty of few tens of nanometres. The resulting clouds of points are then associated to theoretical model at the same level of accuracy so as to obtain parameters that indicate about form error. Minimum zone (*MZ*), defined as the least value of peak to valley (*PV*), is widely used to assess form error. Least squares method (L_2) is often used to determine *MZ* but the resulting value is usually overestimated. For this reason, L_2 is replaced by L_∞ norm because it gives a more accurate value of *MZ* since it directly minimizes *PV*. Using L_∞ norm results in a non-smooth optimization problem and consequently its resolution becomes more challenging compared to L_2.

In this paper, a novel minimax fitting method for accurate metrology of aspheres and freeform based on a hybrid trust region algorithm (HTR) is proposed. To assess performance of the introduced method, it was compared to an available minimax fitting algorithm based on a smoothing technique: exponential penalty function (EPF). The choice of EPF is justified by superior performances in comparison to existing techniques. Comparison was conducted on reference data, data available in literature and data gathered form measurements of a real optical high quality asphere. Results show superiority of HTR over EPF in both returned *PV* values and execution time.

1. Introduction

Aspheres and freeform optics have replaced spherical components in several optical systems due to their superiority over classical (spherical) elements especially for eliminating spherical aberrations [1]. The emergence of new manufacturing techniques such as glass and plastic moulding and grinding as well as polishing methods expands its fields of application in medical imaging, lasers, astronomy, etc. [2].

Form quality of optical aspheres and freeforms is crucial to their performance and functionality. For this reason, form deviations must be tracked all over components' lifetime from design to operational use. Nowadays, available techniques allow manufacturing complex geometries and provide sub-micrometre-level corrections. On the other hand, form assessment of optical elements and data processing still a major issue [3]. Form assessment consists of determining whether form errors are within tolerance specifications. For complex shapes, aspherics for instance, data gathered from ultra-high precision CMMs must be treated in a way to give parameters that indicate about tolerance zone. One of these parameters is usually taken as the peak to valley (*PV*). Therefore, the least value of *PV* which corresponds to the minimum zone (*MZ*) must be determined (Fig. 1).

To determine the *PV*, deviations of data points from a reference surface must be determined *a priori*. There exist several ways to determine the reference surface but the one fitted according to a least squares (L_2) criterion is the widely used [3,4]. The main reason for using L_2 lies in simplicity when solving the resulting minimization problem compared to other criteria. Nevertheless, L_2 usually overestimates *MZ* which causes the rejection of a number of conforming parts. In another way, L_∞ criterion results in a direct minimization of *PV* and consequently returns the closest value of *MZ* to actual.

In this context, a European project 15SIB01-FreeFORM was launched in 2016 to develop reference L_∞ fitting algorithms and traceable metrology for aspheres and freeform optical lenses with below 30 nm accuracy [5].

In general, minimum zone determination problem could be mathematically formulated as follows:

$$\min_{\boldsymbol{x}} \phi(\boldsymbol{x}) \text{ where } \phi(\boldsymbol{x}) = \max_{1 \leqslant i \leqslant m} f_i(\boldsymbol{x}) \text{ and } \boldsymbol{x} = \{\boldsymbol{T}, \boldsymbol{s}\} \quad (1)$$

f_i is the Euclidean distance between the measured point (P_i) and its corresponding projection into the surface (Q_i), $\boldsymbol{x} \in R^n$ could be either the set of intrinsic shape parameters $\boldsymbol{s}$, or the motion parameters $\boldsymbol{T}$:

* Corresponding authors at: Laboratoire Commun de Métrologie (LCM), Laboratoire National de Métrologie et d'Essais (LNE), 1 Rue Gaston Boissier, 75015 Paris, France (Y. Arezki).
E-mail addresses: yassir.arezki@lne.fr (Y. Arezki), hichem.nouira@lne.fr (H. Nouira).

https://doi.org/10.1016/j.measurement.2018.05.071
Received 28 July 2017; Received in revised form 16 May 2018; Accepted 19 May 2018
Available online 21 May 2018

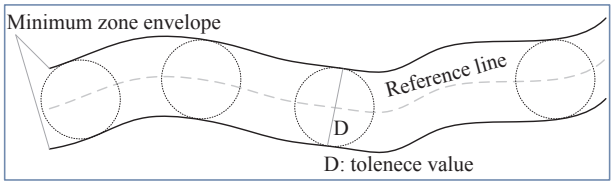

Fig. 1. Tolerance zone definition.

rotation and translation applied to $\{P_i\}$.

Even that L_∞ criterion gives a smaller value of *PV*, the formulated objective function is non-differentiable and the resulting problem is very difficult to solve since a wide range of derivative-based techniques could not be used.

The choice of a mathematical formulation to describe the aspheric is also crucial because it affects the obtained *MZ*. Although there exist several formulations to describe an aspheric lens: splines, Chebyshev polynomials, Zernike polynomials, etc. [6]. The one given by ISO 10110-Part 12:2007 [7] called monomial formulation is the most used. Its mathematical expression is presented in (2).

$$z(r) = \frac{r^2}{R\left(1 + \sqrt{1-(1+\kappa)\frac{r^2}{R^2}}\right)} + \sum_{m=0}^{M} a_{2m+4} r^{2m+4} \tag{2}$$

Where:

$z \rightarrow$ sag of surface
$r \rightarrow$ radial distance
$R \rightarrow$ radius of curvature
$\kappa \rightarrow$ conic constant
$a_{2m+4} \rightarrow$ monomial coefficients

The aperture size of the lens R_{max} defines the domain of r: $0 \leqslant r \leqslant R_{max}$ for which Eq. (2) is valid. The number of monomial terms M depends on the targeted accuracy. Despite its simplicity, this formulation represents some serious drawbacks especially those due to its numerical instability. Thus, when performing L_2 fitting, the resulting Gram matrix is usually ill-conditioned, which outcomes in less accuracy because of significant loss of digits. Other formulations were proposed to cope with these drawbacks. They consist of using orthogonal polynomials instead of monomials [8]. As consequence, the obtained Gram matrix is nearly diagonal and the resulting system is more stable.

This paper is structured as follows. In Section 2, an overview of minimum zone fitting methods is presented. In Section 3, the implementation of the hybrid trust region (HTR) algorithm is detailed. Validation of HTR against EPF is carried out on generated reference data as well as benchmark data in Section 4. In the last section, an investigation of a real case study of a measured high quality optical asphere is illustrated.

2. Literature review

Minimum zone determination for classical geometries such as lines, planes, circles and spheres has been extensively studied and different methods were developed [9]. Computational geometry techniques were used in [10–15] to determine minimum zone for straightness, flatness, circularity, cylindiricity and sphericity tolerance. This class of methods represent a major advantage since no derivative calculations are required. Furthermore, they can find the exact solution but their use is restricted to simple geometries and could not be extended to freeforms. Another free derivative method based on downhill simplex algorithm was proposed to determine straightness tolerance [16,17]. Genetic algorithms were also used for form error determination [18–20].

In regards to freeform shapes, many methods were developed for minimum zone assessment. A first approach makes use of L_p norm [21]. At each iteration the value of p is incremented and the corresponding L_p based smooth objective function is minimized using classical methods until a termination criterion is satisfied. This method suffers from serious instability especially when approaching the optimal solution because the resulting L_p based objective function becomes nearly non-differentiable. A heuristic method based on differential evolution algorithm (DE) was recently developed for freeforms [22]. This method performs poorly especially with large clouds of data points. Moreover, given results are not deterministic.

In order to make use of differentiation optimization techniques, the aggregation function method could be used. In [23,24], an exponential penalty function (EPF) is used to approximate the non-smooth objective function via a twice differentiable one. The resulting function could be minimized using Newton based method or any derivative-based optimization technique. This method gives good results but represents some instabilities due to exponential terms.

The minimum zone determination problem could be formulated as a nonlinear constrained problem. The formulation were detailed in [25], and a primal-dual interior point algorithm (PDIP) was implemented to solve the resulting problem. This method represents lower performances compared to EPF since minimization of the resulting Lagrangian function requires the resolution of large linear systems with ill-conditioned matrices.

3. Hybrid trust region algorithm (HTR)

The main idea of the hybrid trust region algorithm consists of performing either trust region step, line search step or curve search step according to the specific situation faced at each iteration [26,27]. It enables to avoid solving the trust region problem many times. For every iteration, a first stage consists of obtaining a trust region trial step d_k by solving the quadratic problem given in (3).

$$QP(x_k,\boldsymbol{B_k}): \begin{cases} \min_{(d,z)\in R^{n+1}} \frac{1}{2} < d,\boldsymbol{B_k} d > + z = M_k(d,z), \\ s.\ t. < \nabla f_i(x_k),d > -z \leqslant \phi(x_k) - f_i(x_k), i = 1,...,m \\ \|d\|_\infty \| \leqslant \Delta_k \end{cases} \tag{3}$$

where $\boldsymbol{B_k}$ is n by n symmetric positive definite matrix, Δ_k is the parameter defining the trust region domain, z is an introduced parameter depending on the first derivative of the objective function ϕ, ∇f_i is the gradient of the function f_i and $'' < . ,. > ''$ denotes the dot product.

The trust region domain is defined using L_∞ instead of L_2 so as *QP* becomes an easily-solved quadratic problem. It should be mentioned that the proposed *QP* in (3) has always a solution since (0,0) lies inside the feasible domain. This problem could be solved using classical methods adapted to quadratic problems such as interior point method [28].

If the resulting trust region trial step d_k could not be accepted, a corrected step $d_k + \widetilde{d}_k$ is determined by solving the problem in (4).

$$\widetilde{QP}(x_k,\boldsymbol{B_k}): \begin{cases} \min_{(\widetilde{d},\widetilde{z})\in R^{n+1}} \frac{1}{2} < d_k + \widetilde{d}, \boldsymbol{B_k}(d_k + \widetilde{d}) > + \widetilde{z} = \widetilde{M}_k(\widetilde{d},\widetilde{z}), \\ s.\ t. < \nabla f_i(x_k),\widetilde{d} > -\widetilde{z} \leqslant \phi(x_k + d_k) - f_i(x_k + d_k), i = 1,...,m \\ \|d_k + \widetilde{d}_\infty\| \leqslant \Delta_k \end{cases} \tag{4}$$

If neither the initial trust region step d_k nor the corrected step $d_k + \widetilde{d}_k$ could be acceptable in trust region scheme, a line search along d_k or a curve search is performed if d_k is a descent direction (the actual reduction $r_k > 0$ in (6)). Otherwise ($r_k \leqslant 0$), a curve search is used to find a step length t_k that verifies (5).

$$\phi(x_k + t_k d_k + t_k^2 \widetilde{d}_k) \leqslant \phi(x_k) - \alpha t_k \langle d_k, \boldsymbol{B_k} d_k \rangle \tag{5}$$

where $\alpha \in (0,1/2)$, d_k is the solution of (3) and $\widetilde{d}_k$ is the solution of (4). In the case $\|d_k\| \leqslant \|\widetilde{d}_k\|$, $\widetilde{d}_k$ should be taken to be 0. The implemented algorithm follows the next steps:

- Step 1: Give initial values $x_0 \in R^n, \varepsilon > 0, \Delta_{max}, \Delta_0 \in (0, \Delta_{max}), 0 < \tau_1 < 1 < \tau_2, \alpha \in (0,1/2), \beta \in (0,1/2), 0 < \mu < 2\alpha, \eta \in (0.5,1)$, $\boldsymbol{B}_0 = \boldsymbol{I}$, k: $=0$.
- Step 2: Determine (d_k, z_k) by solving the quadratic problem (3). If $\|d_k\| \leqslant \varepsilon$, stop; Otherwise;
- Step 3: Compute the ratio between the actual reduction and the predicted reduction

$$r_k = \frac{\phi(x_k) - \phi(x_k + d_k)}{M_k(0,0) - M_k(d_k, z_k)} \tag{6}$$

- Step 4: (Update the iteration point)
  (4.1) If $r_k > \mu$, set $s_k = d_k$, $x_{k+1} = x_k + s_k$, go to step 5; Otherwise;
  (4.2) Compute the second-order correction step $\tilde{d}_k$ by solving problem (4), In the case $\|d_k\| \leqslant \|\tilde{d}_k\|$, $\tilde{d}_k$ is set to be 0.
  (4.3) Compute corrected $\tilde{r}_k$

$$\tilde{r}_k = \frac{\phi(x_k) - \phi(x_k + d_k + \tilde{d}_k)}{M_k(0,0) - M_k(d_k, z_k)} \tag{7}$$

  (4.4) If $\tilde{r}_k > \mu$, set $r_k = \tilde{r}_k$, $s_k = d_k + \tilde{d}_k$, $x_{k+1} = x_k + s_k$, go to step 5; Otherwise;
  (4.5) If $r_k > 0$, set $\tilde{d}_k = 0$.
  (4.6) (Perform curve search) Compute t_k: the first number in the sequence of $\{1, \beta, \beta^2, \ldots\}$ to verify (5). Set $s_k = t_k d_k + t_k^2 \tilde{d}_k$ and $x_{k+1} = x_k + s_k$.
- Step 5: (Update Δ_k)
  If $r_k \leqslant \mu$, $\Delta_{k+1} \in [\|s_k\|, \tau_1 \Delta_k]$;
  If $r_k \geqslant \eta$, $\Delta_{k+1} = \min(\tau_2 \Delta_k, \Delta_{max})$;
  Otherwise, $\Delta_{k+1} = \Delta_k$.
- Step 6: (Update $\boldsymbol{B_k}$), Update $\boldsymbol{B_k}$ to $\boldsymbol{B_{k+1}}$; k: $=k+1$, go to step 1.

To update $\mathbf{B_k}$, the Powell's modification of BFGS formula is used [29]. A simplified flowchart of hybrid trust region algorithm is summarized in Fig. 2 and an illustration of the principle of the trust region method is shown in Fig. 3.

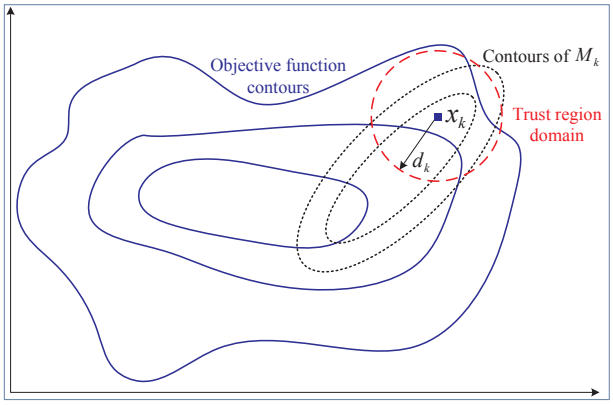

Fig. 3. Illustration of trust region method.

4. Numerical validation

4.1. Application on reference data

A set of reference datasets (softgauges) with previously known *MZ* value (MZ_{ref}) are generated using a method proposed in [30]. The main idea of this method is to state optimality conditions for the problem given in (1) and then derive datasets for which optimality conditions are automatically met. It should be noted that in the case of aspheric shapes, this method could only generate vertex solutions.

For the validation process, only transformation parameters are sought. Surface nominal coefficients are supposed given. Five configurations of coefficients are used (Table 1). These coefficients are chosen in a way to provide different slope values between 5 and 85° at $r = R_{max} = 20$ mm to the nominal aspheric shape. The radius of curvature R varies between 0.75 and 102 mm. The conic constant was given values with the set {−1, −0.9 and −0.8}. For each configuration, data with predefined number of points (N = {121, 1024, 10,404 and 100,489}) and a previously known MZ_{ref} ($MZ_{ref} = 10^{-4}$) are generated.

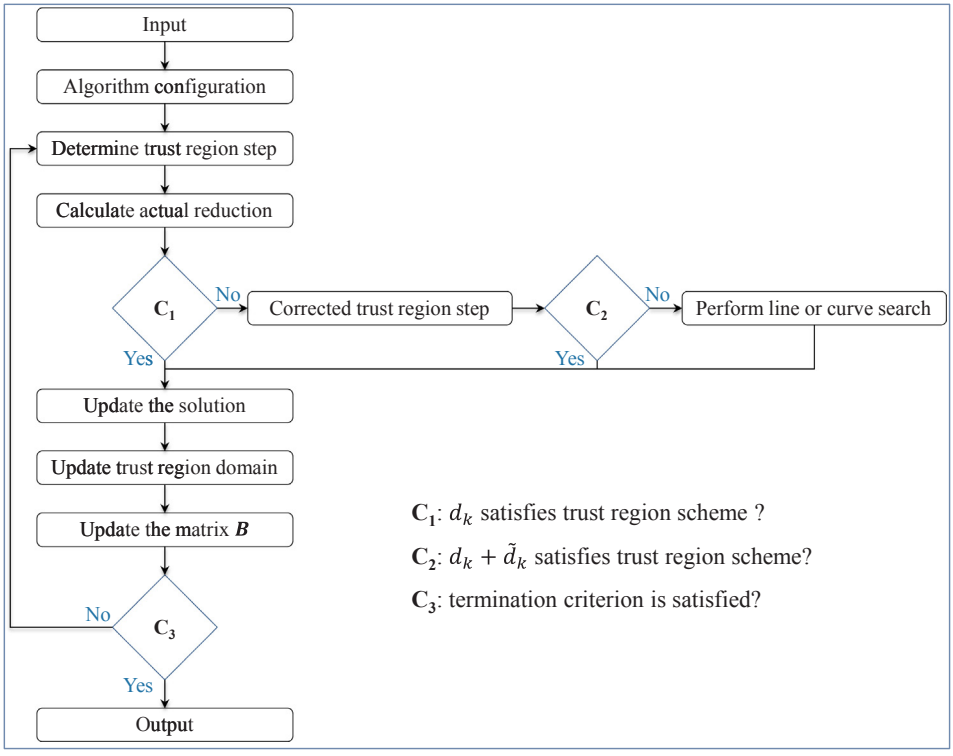

Fig. 2. A simplified flowchart of the hybrid trust region algorithm.

Table 1
Surface nominal coefficients used for reference data generation.

Configuration	Coefficients							
	R (mm)	κ	a_4 (mm^{-3})	a_6 (mm^{-5})	a_8 (mm^{-7})	a_{10} (mm^{-9})	R_{max} (mm)	Slope (°)
I	101.58	−1	$-1.70\ 10^{-13}$	$-8.51\ 10^{-14}$	$-4.25\ 10^{-14}$	$-2.12\ 10^{-14}$	20	5
II	19.79	−0.9	$-1.51\ 10^{-17}$	$-7.55\ 10^{-18}$	$-3.77\ 10^{-18}$	$-1.88\ 10^{-19}$	20	25
III	8.88	−0.8	$-1.94\ 10^{-12}$	$-9.72\ 10^{-13}$	$-4.86\ 10^{-13}$	$-2.43\ 10^{-13}$	20	45
IV	4.14	−0.9	$-4.17\ 10^{-12}$	$-2.08\ 10^{-12}$	$-1.04\ 10^{-12}$	$-5.21\ 10^{-13}$	20	65
V	0.77	−1	$-2.22\ 10^{-11}$	$-1.11\ 10^{-11}$	$-5.56\ 10^{-12}$	$-2.78\ 10^{-12}$	20	85

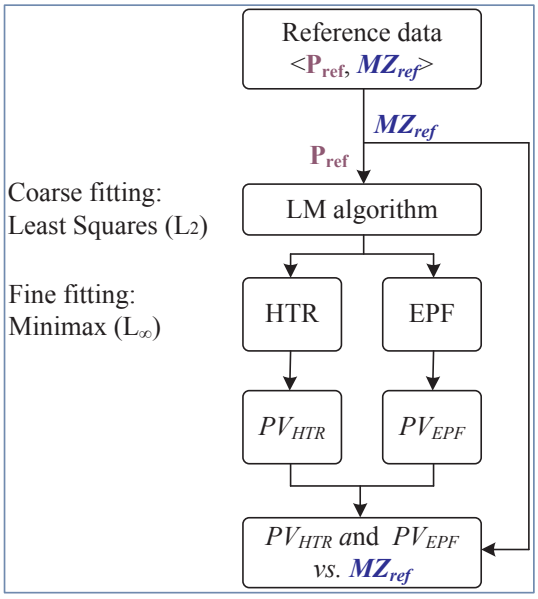

Fig. 4. Comparison methodology.

In order to assess the performance of the algorithm proposed in regards to exponential penalty function algorithm (EPF) [23], each generated dataset were submitted at the same time to both algorithms: EPF and HTR. The corresponding *PV* values respectively PV_{EPF} and PV_{HTR}, as well as execution time, respectively T_{EPF} and T_{HTR}, are compared as described in Fig. 4.

Initial data is rotated by angle $\pi/20$ around x axis and $\pi/15$ around y axis as well as translated by -1 mm in x direction, 1 mm in y direction and -1 mm in z direction (Fig. 5). Both algorithms were implemented on a personal computer based on Intel Core i7/x64 platform with 8 GB of RAM and a 2.40 GHz processor.

Tables 2–4 illustrate obtained values of PV-MZ_{ref} as well as

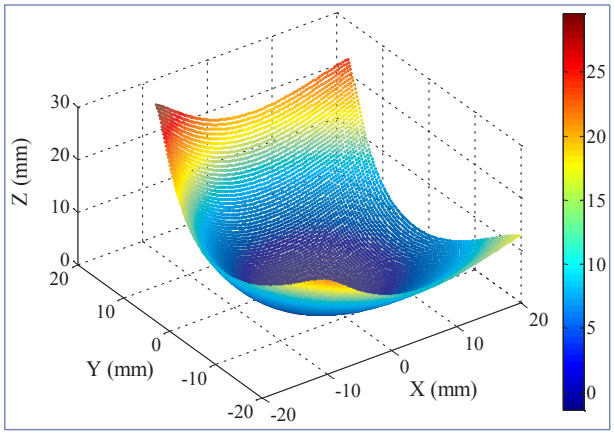

Fig. 5. An example of generated reference data (10 404 points).

Table 2
Values of PV-MZ_{ref} and execution time for HTR and EPF (configuration II).

N	MZ_{HTR}-MZ_{ref} (mm)	MZ_{EPF}-MZ_{ref} (mm)	T_{HTR} (s)	T_{EPF} (s)
121	$4.06\ 10^{-19}$	$1.45\ 10^{-15}$	0.84	2.68
1024	$9.50\ 10^{-16}$	$1.11\ 10^{-16}$	2.07	9.15
10,404	$1.78\ 10^{-16}$	$4.51\ 10^{-13}$	12.1	61.91
100,489	$1.64\ 10^{-16}$	$4.92\ 10^{-15}$	41.51	226.96

Table 3
Values of PV-MZ_{ref} and execution time for HTR and EPF (configuration III).

N	PV_{HTR}-MZ_{ref} (mm)	PV_{EPF}-MZ_{ref} (mm)	T_{HTR} (s)	T_{EPF} (s)
121	$4.24\ 10^{-15}$	$1.13\ 10^{-14}$	2.18	2.48
1024	$2.18\ 10^{-16}$	$2.61\ 10^{-16}$	4.32	4.47
10,404	$1.41\ 10^{-15}$	$3.08\ 10^{-15}$	4.27	36.50
100,489	$6.73\ 10^{-15}$	$6.78\ 10^{-15}$	20.52	255.06

Table 4
Values of PV-MZ_{ref} and execution time for HTR and EPF (configuration IV).

N	PV_{HTR}-MZ_{ref} (mm)	PV_{EPF}-MZ_{ref} (mm)	T_{HTR} (s)	T_{EPF} (s)
121	$4.03\ 10^{-15}$	$9.78\ 10^{-14}$	1.14	1.79
1024	$8.14\ 10^{-16}$	$8.42\ 10^{-15}$	5.23	7.24
10,404	$1.15\ 10^{-16}$	$2.14\ 10^{-15}$	35.88	200.16
100,489	$9.86\ 10^{-15}$	$1.05\ 10^{-14}$	50.03	274.75

execution time for both algorithms. Concerning PV values, both algorithms give enough accurate results with superiority of HTR for all test cases. In average, the relative error between PV values obtained using EPF (resp. HTR) and MZ_{ref} is 10^{-8}% (resp. 10^{-9}%). In fact, for approximately all generated data points, HTR returns PV values ten times more accurate than EPF. In regards to execution time, HTR clearly overcomes EPF. For the latter algorithm, execution time is five times higher than the formal, especially for data points that exceed 1000 points. When multiplying the number of points by 1000, T_{HTR} was multiplied by 50 while T_{EPF} by 150 in their corresponding worst cases.

EPF is a smoothing technique that consists of approximating the non-differentiable objective function by a smooth one at each iteration and then minimizes it. For this aim, Newton method is used so the Hessian matrix must be calculated. Since the Hessian matrix calculation time is proportional to the number of points in the data set, the execution time increases even when considering an active set. Moreover, descent direction determination is not always accurate since the obtained Hessian matrix is not positive definite all the time. Hence, corrections must be brought to the Hessian matrix whenever is needed.

On the other hand, when establishing the *QP* for HTR algorithm, the matrix $\boldsymbol{B}$ is chosen to be symmetric positive definite, the Powell's modification of BFGS formula proves to be efficient for this purpose and there is no need to calculate second order derivation terms, which considerably reduces execution time.

Table 5
Comparison of HTR and EPF on benchmark data (8100 points).

	HTR	EPF
PV (nm)	3.15	3.21
Execution time (s)	2.39	2.34

Fig. 6. Photo of the AO775 aspherical lens.

Fig. 7. Photo of the ultra-high precision Nanomefos measuring machine.

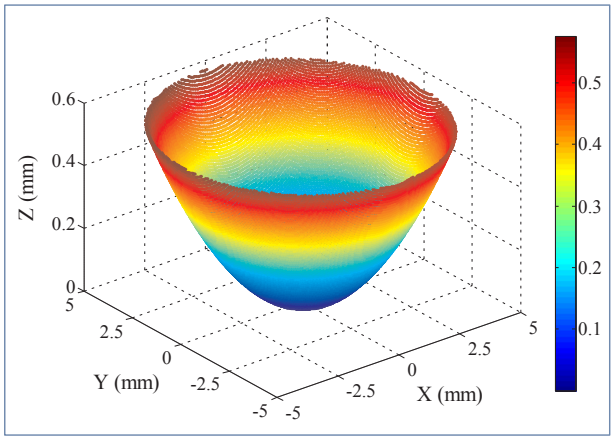

Fig. 8. AO775 optical aspherical lens: measured data using the ultra-high precision Nanomefos machine (31 390 points).

4.2. Application on benchmark data

Data available in literature were also used to assess the result given by the algorithm proposed. We refer to [22] where a heuristic method based on differential evolution algorithm (DE) was developed and a data set of 8100 points were used to verify the algorithm. The nominal coefficients of the aspheric surface are: $R = 520$ mm, $\kappa = -0.7$, $a_4 = 5.210^{-5}$, $a_6 = -6.510^{-6}$, $a_8 = 3.1110^{-8}$, $a_{10} = 3.22210^{-9}$. Fractal Brownian function was used to generate noise with amplitude $\sigma = 1$ μm around the nominal surface. The same data points was adopted for a comparison between EPF and DE in [23].

Table 6
Comparison of HTR, EPF on measured data (31 390 points).

	Least squares (L_2)	Minimax (L_∞)	
		HTR	EPF
PV (nm)	536	470.36	479.43
Execution time (s)	10.23	107.69	586.96

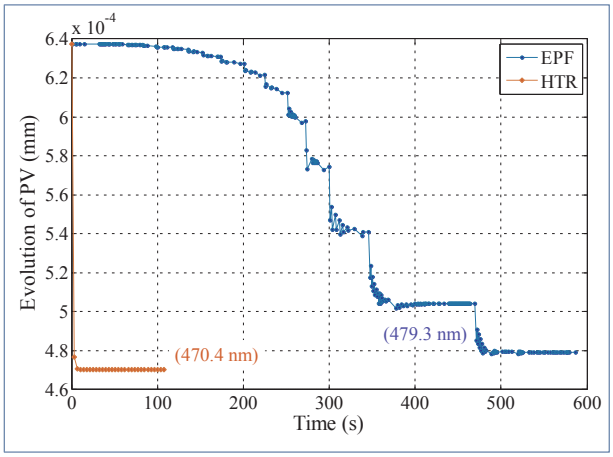

Fig. 9. Evolution of *PV* value for HTR and EPF algorithms applied on measured data (31 390 points).

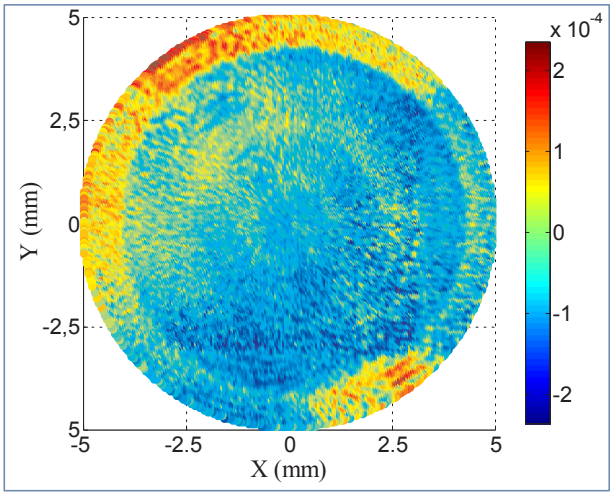

Fig. 10. AO775 optical aspherical lens: residual values (31 390 points).

Table 5 illustrates a comparison of results obtained by EPF and HTR. *PV* value given by the formal algorithm is 3.21 μm. The newly proposed HTR algorithm provides a lower value of 3.15 μm, which is approximately 60 nm lower. A 60 nm difference in result could cause an aspheric lens to be rejected while it is conforming to specifications. In regards to execution time, the two values are approximately similar.

5. Experimental investigation

A high quality optical aspherical lens AO775, manufactured by Anteryon® company using a Single Point Diamond Turning (SPDT) process and finished with a high precision polishing process and glass coating, was selected for test (Fig. 6). The intrinsic parameters of the AO775 asphere are:

- curvature at the apex is equal to $c = 10^{-20}$ mm^{-1},
- conic constant is $\kappa = -1$,
- asphere coefficients are: $a_2 = 0.0223$, $a_4 = 7.29310^{-6}$, $a_6 = 4.5210^{-9}$, $a_8 = -1.06110^{-11}$ and $a_{10} = 9.88710^{-15}$,
- sag $S = 3.217$ mm,
- clear aperture $CA = 11.74$ mm.

The asphere was scanned at the Netherlands Organisation for Applied Scientific Research (TNO) using the ultra-high precision Nanomefos machine (Fig. 7) [31–33], designed specifically for non-contact measurement of aspherical and freeform optics. As these surfaces are in general rotationally symmetric, the Nanomefos machine has a cylindrical setup resulting in less moving axes and higher measurement speed compared to orthogonal setup machines. To be able of measuring slopes from -45° concave to +45° convex, the optical probe can be tilted such that it is perpendicularly aligned to the best-fit asphere of the surface.

The measurement uncertainty is mainly determined by the metrology loop between the probe and the artefact. It was evaluated to about 10 nm when the probe is perpendicular to the surface under test. Further details about the Nanomefos machine are presented in [32,33].

The selected AO775 optical asphere was mounted on the air bearing table and scanned using the non-contact probe system. A set of 31 390 points was collected, as shown in Fig. 8, and analysed using the implemented minimax EPF and HTR fitting algorithms.

Table 6 illustrates results obtained using HTR and EPF as well as *PV* values given by L_2 fitting. HTR provides more accurate result than EPF since PV_{HTR} (470.36 nm) is approximately 9 nm lower than PV_{EPF} (479.43 nm). This value could be considered as too high when targeting uncertainty at the nanometre level.

Furthermore, *PV* value given by L_2 (536 nm) is considerably higher than both other values with a difference of 66 nm which confirms the statement, made in the introduction, that L_2 overestimates *MZ*. Similarly to reference data, EPF takes approximately five times execution time than HTR. Fig. 9 shows the evolution of *PV* values obtained using EPF and HTR in function of execution time. It illustrates the rapidity of HTR to converge compared to EPF. The final residuals obtained using HTR is presented in Fig. 10. For all the above reasons, superiority of the new implemented fitting method for aspheres and freeforms minimax fitting is proved.

6. Conclusion

Unlike L_2, minimax fitting can exactly estimate form error by directly minimizing the peak to valley (*PV*). Obtaining the exact minimum zone for profile or surface tolerance could be achieved at the expense of facility of the resulting mathematical formulation of the problem.

In this paper, a novel method for minimax fitting of complex geometries was developed. This method is based on a Hybrid Trust Region algorithm (HTR). This newly proposed algorithm consists of a combination of a classical trust region method and a line search or curve search depending on the situation faced. In order to assess the performance of this algorithm against available ones, the novel algorithm was compared to exponential penalty function algorithm (EPF) based on a smoothing technique for minimizing non-smooth objective function.

The implemented HTR algorithm was first tested and validated using generated reference data sets. Softgauges generation was conducted in a way to obtain several shapes that simulate different conditions (number of points, form error and slope). Initial results show superiority of HTR over EPF in terms of obtained *PV* values and execution time. This result was confirmed, in a second step, when analysing benchmark data available in literature.

A high quality optical asphere was selected for experimental investigation. It was scanned using the ultra-high precision Nanomefos measuring machine. A set of 31 390 points was recorded and submitted to the two compared algorithms. Once again, results show superiority of HTR over EPF in both resulting minimum zone values and execution time.

Acknowledgements

The authors sincerely thank the EMPIR organization. The EMPIR initiative is co-funded by the European Union's Horizon 2020 and innovation programme and the EMPIR participating states within EURAMET and the European Union (15SIB01: FreeFORM). Authors would like also to thank Dr. Xiangchao Zhang from Fudan University and Dr. Rens Henselmans from TNO for providing simulated and measured datasets and all partners from: CMI, PTB, SMD, TUBITAK, VTT, ENS-Cachan, FU, GEOMNIA, POLYU, UnB.

References

[1] J.M. Geary, *Introduction to Lens Design: With Practical ZEMAX Examples*, Willmann-Bell, 2002.
[2] H.H. Karow, Fabrication Methods for Precision Optics, Wiley, 2004.
[3] N. El-Hayek, H. Nouira, N. Anwer, O. Gibaru, M. Damak, A new method for aspherical surface fitting with large-volume datasets, Precis. Eng. 38 (4) (Oct. 2014) 935–947.
[4] D.J. Whitehouse, Surfaces and their Measurement, Elsevier, 2004.
[5] FreeFORM: Home. [Online]. Available: https://www.ptb.de/empir/freeform-home.html. [Accessed: 19-Jun-2017].
[6] H. Gross et al. Overview on surface representations for freeform surfaces. In: SPIE; 2015:vol. 9626.
[7] ISO 10110-Part12. Optics and photonics – Preparation of drawings for optical elements and systems – Part 12: Aspheric surfaces; 2007.
[8] G.W. Forbes, Shape specification for axially symmetric optical surfaces, Opt. Express 15 (8) (Apr. 2007) 5218–5226.
[9] H. Nouira, P. Bourdet, Evaluation of roundness error using a new method based on a small displacement screw, Meas. Sci. Technol. 25 (4) (2014) 25.
[10] G.L. Samuel, M.S. Shunmugam, Evaluation of straightness and flatness error using computational geometric techniques, Comput.-Aided Des. 31 (13) (Nov. 1999) 829–843.
[11] G.L. Samuel, M.S. Shunmugam, Evaluation of circularity from coordinate and form data using computational geometric techniques, Precis. Eng. 24 (3) (Jul. 2000) 251–263.
[12] G.L. Samuel, M.S. Shunmugam, Evaluation of sphericity error from form data using computational geometric techniques, Int. J. Mach. Tools Manuf. 42 (3) (Feb. 2002) 405–416.
[13] N. Venkaiah, M.S. Shunmugam, Evaluation of form data using computational geometric techniques—Part II: Cylindricity error, Int. J. Mach. Tools Manuf. 47 (7) (Jun. 2007) 1237–1245.
[14] N. Venkaiah, M.S. Shunmugam, Evaluation of form data using computational geometric techniques—Part I: Circularity error, Int. J. Mach. Tools Manuf. 47 (7) (Jun. 2007) 1229–1236.
[15] G. Hermann, G. Hermann. Application of computational geometry in coordinate measurement. In: 2015 IEEE 10th Jubilee International Symposium on Applied Computational Intelligence and Informatics, 2015, pp. 511–516.
[16] E. Orady, S. Li, Y. Chen, Evaluation of minimum zone straightness by a nonlinear optimization method, J. Manuf. Sci. Eng. 122 (4) (Jun. 1999) 795–797.
[17] S. Cho, J.-Y. Kim, Straightness and flatness evaluation using data envelopment analysis, Int. J. Adv. Manuf. Technol. 63 (5–8) (Nov. 2012) 731–740.
[18] X. Wen, A. Song, An immune evolutionary algorithm for sphericity error evaluation, Int. J. Mach. Tools Manuf. 44 (10) (Aug. 2004) 1077–1084.
[19] X. Wen, A. Song, An improved genetic algorithm for planar and spatial straightness error evaluation, Int. J. Mach. Tools Manuf. 43 (11) (Sep. 2003) 1157–1162.
[20] A. Rossi, M. Antonetti, M. Barloscio, M. Lanzetta, Fast genetic algorithm for roundness evaluation by the minimum zone tolerance (MZT) method, Measurement 44 (7) (Aug. 2011) 1243–1252.
[21] Y.G. Shi, Weighted simultaneous Chebyshev approximation, J. Approx. Theory 32 (4) (1981) 306–315.
[22] X. Zhang, X. Jiang, P.J. Scott, A minimax fitting algorithm for ultra-precision aspheric surfaces, J. Phys. Conf. Ser. 311 (1) (2011) 012031.
[23] X. Zhang, H. Zhang, X. He, M. Xu, X. Jiang, Chebyshev fitting of complex surfaces for precision metrology, Measurement 46 (9) (Nov. 2013) 3720–3724.
[24] Y. Arezki, X. Zhang, C. Mehdi-Souzani, N. Anwer, H. Nouira, Investigation of minimum zone assessment methods for aspheric shapes, Precis. Eng (2018).
[25] X. Zhang, X. Jiang, A.B. Forbes, H.D. Minh, P.J. Scott, Evaluating the form errors of spheres, cylinders and cones using the primal–dual interior point method, Proc. Inst. Mech. Eng. Part B J. Eng. Manuf. 227 (5) (May 2013) 720–725.
[26] F. Wang, K. Zhang, A hybrid algorithm for nonlinear minimax problems, Ann. Oper. Res. 164 (1) (Nov. 2008) 167.
[27] F. Wang, C. Wang, L. Wang, A new trust-region algorithm for finite minimax problem, J. Comput. Math. 30 (3) (2012) 262–278.
[28] S.P. Boyd, L. Vandenberghe, Convex Optimization, Cambridge University Press, 2004.

[29] M.J.D. Powell, How bad are the BFGS and DFP methods when the objective function is quadratic? Math. Program. 34 (1) (Jan. 1986) 34–47.
[30] A.B. Forbes, H.D. Minh, Form Assessment in Coordinate Metrology, SpringerLink, 2011, pp. 69–90.
[31] R. Henselmans, L.A. Cacace, G.F.Y. Kramer, P.C.J.N. Rosielle, M. Steinbuch, The NANOMEFOS non-contact measurement machine for freeform optics, Precis. Eng. 35 (4) (Oct. 2011) 607–624.
[32] R. Henselmans, Non-contact measurement machine for freeform optics, Technische Universiteit Eindhoven, Eindhoven, 2009.
[33] H. Nouira, R.H. Bergmans, A. Küng, H. Piree, R. Henselmans, H.a.M. Spaan, Ultra-high precision CMMs and their associated tactile or/and optical scanning probes, Int. J. Metrol. Qual. Eng. 5 (2) (2014) 204.